Neuron, Vol. 30, 369–383, May, 2001, Copyright ©2001 by Cell Press

Axon-Glia Interactions and the Domain Organization of Myelinated Axons Requires Neurexin IV/Caspr/Paranodin

Manzoor A. Bhat,[1,5] Jose C. Rios,[2] Yue Lu,[4] German P. Garcia-Fresco,[1] William Ching,[2] Mary St. Martin,[2] Jingjun Li,[1] Steven Einheber,[2] Mitchell Chesler,[3] Jack Rosenbluth,[3] James L. Salzer,[2,6] and Hugo J. Bellen[4,6]

[1]Cardiovascular Research Institute
Department of Medicine
Department of Biochemistry and Molecular Biology
Mount Sinai School of Medicine
New York, New York 10029

[2]Department of Cell Biology

[3]Department of Physiology and Neuroscience
and Rusk Institute
New York University School of Medicine
New York, New York 10016

[4]Howard Hughes Medical Institute
Department of Molecular and Human Genetics
Program in Developmental Biology
Baylor College of Medicine
Houston, Texas 77030

Summary

Myelinated fibers are organized into distinct domains that are necessary for saltatory conduction. These domains include the nodes of Ranvier and the flanking paranodal regions where glial cells closely appose and form specialized septate-like junctions with axons. These junctions contain a *Drosophila* Neurexin IV-related protein, Caspr/Paranodin (NCP1). Mice that lack NCP1 exhibit tremor, ataxia, and significant motor paresis. In the absence of NCP1, normal paranodal junctions fail to form, and the organization of the paranodal loops is disrupted. Contactin is undetectable in the paranodes, and K^+ channels are displaced from the juxtaparanodal into the paranodal domains. Loss of NCP1 also results in a severe decrease in peripheral nerve conduction velocity. These results show a critical role for NCP1 in the delineation of specific axonal domains and the axon-glia interactions required for normal saltatory conduction.

Introduction

The ability of myelinated axons to conduct action potentials by saltatory conduction depends on the distribution of numerous molecular components, notably voltage-gated ion channels, into distinct domains. These domains—the internode, the paranodal and juxtaparanodal regions, and the node of Ranvier—form as the result of specific interactions between axons and myelinating glial cells, e.g., Schwann cells in the PNS and oligodendrocytes in the CNS (Peles and Salzer, 2000). The molecular composition of these domains and the nature of the axon-glia interactions that are required for their formation are poorly understood.

Voltage-gated sodium (Na^+) channels are highly concentrated at the nodes of Ranvier, whereas delayed rectifier potassium (K^+) channels are localized to the juxtaparanodes. A series of cytoplasmic loops of the glial cells are interposed between these domains and flank the nodes of Ranvier. These glial loops spiral tightly around and form specialized septate-like junctions with the axon (Figure 1A, see schematic). In electron micrographs of longitudinal sections of myelinated axons, the paranodal junctions display periodic intercellular transverse bands. These junctions have several proposed functions: anchoring the paranodal loops to the axon, providing an ion diffusion barrier into the periaxonal space that prevents current loss, and serving as a physical barrier that maintains distinct axonal domains (Rosenbluth, 1995).

Support for the role of these junctions in domain organization has emerged from studies of *ceramide galactosyl transferase* (*CGT*) mutant mice (Bosio et al., 1998; Coetzee et al., 1996). *CGT* mutant mice are unable to synthesize galactocerebroside and sulfatide, two abundant myelin glycolipids. These mice display a variety of paranodal and nodal abnormalities, including absence of the transverse bands—the hallmark of the paranodal junctions (Dupree et al., 1999). Although the mechanisms underlying the paranodal defects in these mice are not understood (Dupree and Popko, 1999), the observation that K^+ channels are mislocalized in these mice (Dupree et al., 1999) suggested that the paranodal junctions play a key role in the delineation of channel domains.

The first molecular constituent of the paranodal junctions to be identified was the rat contactin-associated protein, Caspr (Einheber et al., 1997). This protein was independently identified and localized to these junctions and named Paranodin (Menegoz et al., 1997). Caspr/Paranodin exhibits significant homology in its ectodomain to Neurexins I, II, and III (Missler and Südhof, 1998) but is more similar to *Drosophila* Neurexin IV (NRX IV) (Baumgartner et al., 1996) and Caspr2 (Poliak et al., 1999). Hence, NRX IV and Caspr/Paranodin constitute a subfamily of Neurexin-like proteins referred to as NCPs (Bellen et al., 1998); we will refer to Caspr/Paranodin as NCP1. *Drosophila* NRX IV has been localized to pleated septate junctions of epithelial and glial cells. These junctions display a ladder-like electron-dense structure and are crucial to the integrity of the blood-nerve barrier in *Drosophila* (Baumgartner et al., 1996).

Biochemical studies have shown that NCP1 associates in *cis* with the GPI-anchored neural cell adhesion molecule contactin (Peles et al., 1997). Contactin is required for the surface expression of NCP1 (Faivre-Sarrailh et al., 2000) and both proteins form a high molecular weight complex in the paranodal junctions (Rios et al., 2000). The glial ligands for NCP1 or contactin in the paranodes have not been established. A potential candidate is the 155 kDa isoform of neurofascin, which is expressed by myelinating glia in the paranodal region

[5]Correspondence: bhatm01@doc.mssm.edu
[6]These authors contributed equally to this work.

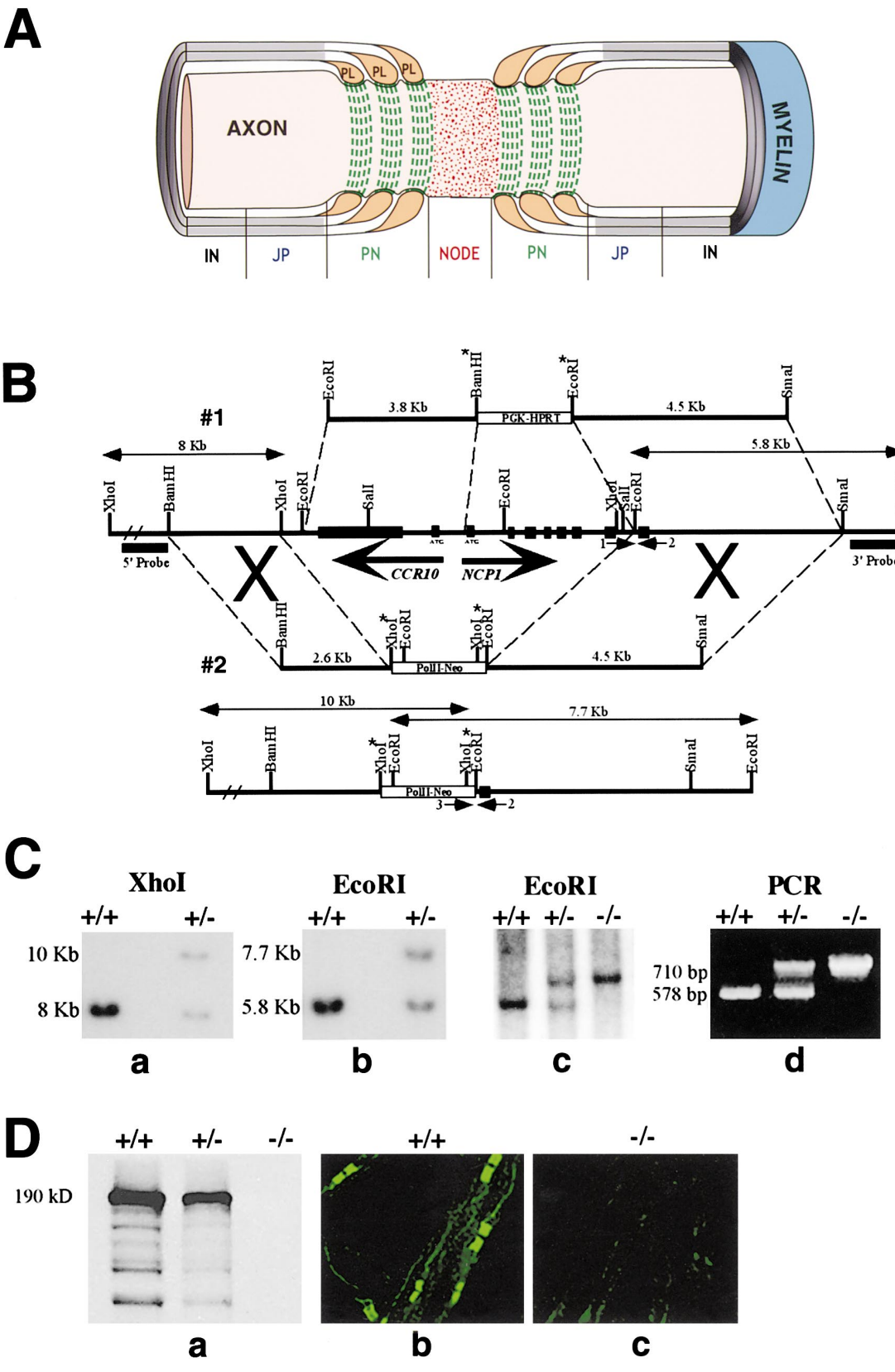

Figure 1. Disruption of *NCP1*

(A) Schematic organization of the various domains of myelinated axons. Domains include the node of Ranvier (Node), the paranodal region (PN), the juxtaparanodal region (JP), and the internode (IN). The axon is surrounded by membranes of a myelinating glial cell, including the

(Davis et al., 1996; Collinson et al., 1998; Tait et al., 2000). Based on the paranodal abnormalities of the *CGT* mutant mice, galactocerebroside and sulfatide may also be considered potential glial ligands.

In this study, we address the role of mouse NCP1 in the formation and function of paranodal junctions. We show that loss of NCP1 in mice causes severe neurologic defects and aberrant organization, and axo-glial interactions in the paranodal region. In addition, the strict separation between Na^+ channels at the node and K^+ channels at the juxtaparanode is abolished and nerve conduction velocity is substantially reduced in the absence of NCP1. Hence, NCP1 plays a key role in the formation of the paranodal junctions and is required for normal saltatory conduction.

Results

Cloning of the Mouse *NCP1* Gene and Generation of Null Mutants

Human Neurexin IV sequences were identified through database searches using the *Drosophila neurexin IV* (*nrx IV)* sequence. One of the human ESTs was used to screen a mouse embryonic cDNA library and overlapping clones were isolated, sequenced, and compiled as a cDNA sequence of 4496 base pairs (accession number AF039833). This sequence contains an open reading frame (ORF) of 1385 amino acids (~153 kDa) with 93% identity to rat Caspr/Paranodin (Menegoz et al., 1997; Peles et al., 1997) and is named NCP1 (Bellen et al., 1998). NCP1 contains an amino-terminal discoidin domain, a laminin G domain, two Neurexin domains, and a PGY-enriched segment in the extracellular region. The cytoplasmic domain contains a band 4.1 binding motif and a proline-rich sequence with at least one consensus SH3 domain binding site. In contrast to *Drosophila* NRX IV and Caspr2, NCP1 lacks a PDZ binding domain consensus sequence at its carboxyl terminus (Baumgartner et al., 1996; Poliak et al., 1999; Bhat et al., 1999).

Using the *NCP1* cDNA as a probe, we cloned and mapped ~30 kb of genomic DNA (Figure 1B). Based on a partial intron-exon structure of the *NCP1* locus, a targeting construct was designed to delete the first 7 exons, or 327 N-terminal amino acids. A *pgk-HPRT* resistance cassette was flanked by a 3.8 kb EcoRI-BamHI fragment (5′ homology) and a 4.5 kb EcoRI-SmaI fragment (3′ homology) (Figure 1B, #1). The linearized targeting vector was electroporated into ES cells, but none of the ES cells survived the drug selection. Drug resistance tests using targeting constructs with the *pgk-HPRT* resistance cassette showed that the *HPRT* gene was not expressed when inserted downstream of the 3.8 kb EcoRI-BamHI fragment (data not shown). The failure of this targeting construct prompted us to design a new targeting vector. This second targeting construct contained a *pol II-neo* resistance cassette flanked by a 2.6 kb BamHI-XhoI fragment (5′ homology) and a 4.5 kb EcoRI-SmaI (3′ homology) (Figure 1B, #2). Upon recombination, this construct deletes the first 7 exons of *NCP1* and the putative regulatory sequences. The linearized targeting vector was electroporated into ES cells, and clones carrying the targeted allele were isolated (Figures 1Ca and 1Cb). These clones were injected into mouse blastocysts, and a chimeric male was obtained that transmitted the targeted allele to its progeny. Heterozygous and homozygous mice were confirmed by genomic Southern analysis and PCR amplification (Figures 1Cc and 1Cd).

Subsequent sequence analysis of the 5′ regulatory region of *NCP1* revealed that the gene encoding chemokine receptor 10 (CCR10), also named G protein coupled receptor 2 (GPR2) (Bonini and Steiner, 1997), is in close proximity to *NCP1* (Figure 1B, left arrow). The initiation codon of *CCR10* gene is separated from that of the *NCP1* gene by ~800 bp and is transcribed in the opposite

compact myelin sheath (Myelin), which opens up into a series of noncompacted paranodal loops (PL) that closely appose and indent the axon. The specialized paranodal junctions, represented by the green dashed lines, form between PL and the axon; these junctions flank the Node that contains a high concentration of sodium channels (red particles).

(B) *NCP1* targeting vector. A restriction map of ~30 kb genomic DNA containing the 5′ region of the *NCP1* gene and a partial intron-exon structure. The exons are represented as black boxes and arrows under the genomic map indicate direction of transcription of two genes: *NCP1* and *CCR10*. A targeting vector was constructed by flanking a *pgk-HPRT* resistance cassette with genomic fragments shown in #1. This construct was designed to delete the first 7 exons of the *NCP1* gene but failed to produce any resistant ES clones because of the silencing of the *pgk-HPRT* resistance marker by the 5′ homology fragment. Another targeting construct was therefore designed with a *pol II-neo* resistance cassette (#2) flanked by genomic fragments that should delete the first 7 exons of the *NCP1* gene, including the 5′ regulatory sequences. This construct produced a targeted allele disrupting the *NCP1* gene but also affected the *CCR10* gene. The *CCR10* gene is transcribed in the opposite orientation and is separated from *NCP1* by ~800 bp. The numerical numbers 1–3 with small arrows indicate the PCR primers used for genotyping. The restriction fragment lengths that will differentiate the targeted allele from wild-type are shown between arrows on top of the restriction enzymes (see also Figures 1Ca–1Cc). The DNA fragments used as the 5′ and 3′ probes to confirm homologous recombination are indicated under the map as black bars. The restriction enzyme sites that were either filled in during cloning or are incapable of restriction digestion are shown with asterisks. The breaks in the 5′ end of the map indicate longer fragment sizes than shown.

(C) Genotyping. Southern hybridization of ES cell genomic DNA digested with XhoI (Ca) and EcoRI (Cb) with probes indicated in (B), and mouse genomic DNA (Cc) using two external probes for 5′ end (Ca) and 3′ end (Cb and Cc). Genotyping by PCR used three primers. Two primers (1 and 2, see [B]) were directed against wild-type sequences to amplify a 578 bp fragment representing the wild-type allele, and one primer against the *neo* sequence (3, see [B]) with primer 2 to amplify a 710 bp fragment representing the mutant allele. The heterozygous animals amplify both fragments.

(D) NCP1 expression. The protein lysates were prepared from brains of wild-type, heterozygous, and homozygous animals and processed for immunoblotting. The wild-type and heterozygous animals showed a predominant protein band migrating at 185–190 kDa that was not detected from homozygous animals demonstrating the loss of the NCP1 protein in *NCP1* mutant mice (Da). Immunohistochemical analysis of sciatic nerves from heterozygous animals showed normal expression of NCP1 at the paranodal junctions (Db), whereas the nerve fibers from homozygous animals did not reveal any immunostaining (Dc). The intensity of the green color in (Dc) was enhanced to reveal the background of nerve fibers.

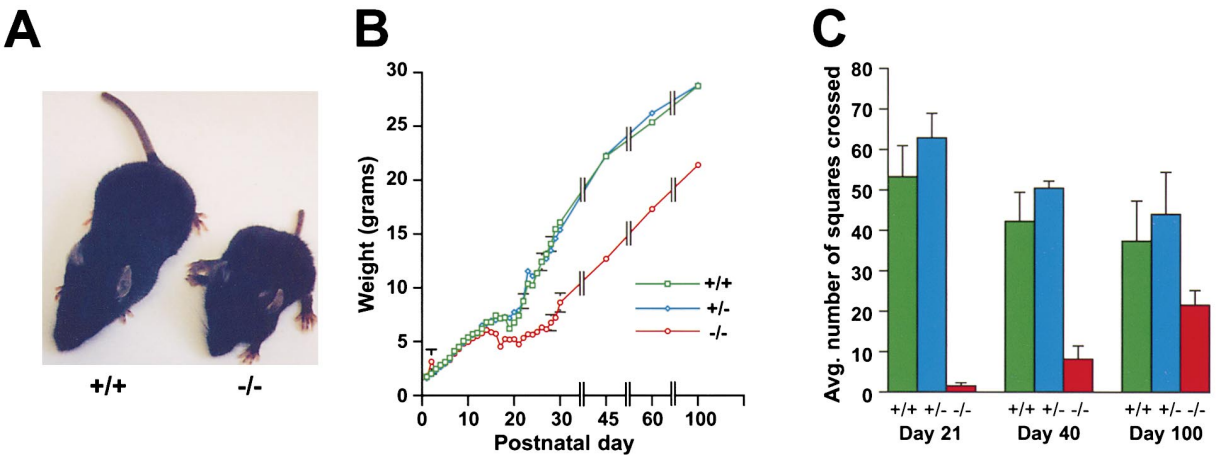

Figure 2. Phenotype of *NCP1* Mutant Mice

(A) Appearance of *NCP1* mutant mice. Wild-type (on left) and *NCP1* mutant (on right) littermates at day 35 are shown; the *NCP1* mutant mouse is approximately half the weight (8 g versus 17 g) of the wild-type mouse and also exhibits a characteristic wide base in the hind limbs.

(B) Weight charts. The chart illustrates the weights of wild-type (+/+), heterozygous (+/−) and homozygous (−/−) male littermates. Wild-type and heterozygous mice were weaned at P19; homozygous mice were left with their mothers.

(C) Motor activity in open field tests. The number of 5 cm × 5 cm squares crossed by each mouse was recorded over a one minute period at P21, P40, and P100. At all times examined, the *NCP1* mutant mice were hypomotile compared to their heterozygous and wild-type littermates although the activity improves at later developmental time points.

orientation. This indicated that the *CCR10* gene is nested within the *NCP1* 5′ regulatory region and is also affected in the *NCP1* mutant mice. Northern blot and RT-PCR analysis have shown that the *CCR10* gene is expressed in the small intestine, colon, and Peyer's patches and that it is not expressed in the nervous system (Jarmin et al., 2000, Homey et al., 2000). In addition, *CCR10* mutant mice have been generated and these mice are healthy, fertile, and do not show any neurologic abnormalities (C. Gerard, personal communication). These results indicate that loss of *CCR10* does not contribute to the neurologic phenotype displayed by the *NCP1* mutant mice (see below).

Mice homozygous for the mutant allele are born at the expected Mendelian frequency from heterozygous intercrosses. The following data indicate that the *NCP1* mutation is a null mutation. First, the NCP1 protein was not detected in whole brain and sciatic nerve homogenates from homozygous mutant mice by Western blot analysis using two independent anti-sera generated to the C-terminal domain of NCP1; the same antisera revealed the 185–190 kDa NCP1 protein in wild-type tissues (Figure 1Da). Second, the NCP1 protein could not be detected by immunohistochemical analysis of mutant sciatic nerves (Figure 1Dc) or in the CNS (see below), whereas wild-type or heterozygous littermates showed strong expression in the paranodal regions (Figure 1Db). Taken together these data show that we have generated a complete loss-of-function of *NCP1*.

NCP1 Mutant Mice Display Severe Neurologic Defects

The *NCP1* mutant mice are indistinguishable from their wild-type littermates until approximately postnatal day 10 (P10). Starting at P11, the mice become identifiable by their smaller stature and progressive neurologic defects that reach maximal severity in the third postnatal week (Figures 2A and 2B; see the video file for behavioral phenotype [http://www.neuron.org/cgi/content/full/30/2/369/DC1]). The defects include hypomotility, a tremor that is accentuated with movement and a wide-based gait suggestive of a cerebellar defect. These mice cannot maintain their balance on a stationary beam and are nearly immobile in open field tests (Figure 2C). They also exhibit generalized motor paresis that is worse in the lower extremities and are unable to support their weight against gravity, climb ropes, or hold onto the edge of the cage. The mutant mice also exhibit occasional extensor spasms of the lower extremities and a hunchback appearance. Most of the mutant mice die at weaning (P21) or shortly thereafter (up to P33), possibly reflecting impaired feeding and maternal care. Removal of wild-type and heterozygous littermates from the cage significantly improves survival but does not alter the neurologic phenotype. These mice slowly increase in size and, in the case of males, approach the weight of their wild-type littermates (Figure 2B). The tremors, hypomotility, and weakness improve slightly (Figure 2C) but then worsen after about 5 months of age. At all ages, heterozygotes appear normal.

Compact Myelin Formation in *NCP1* Mutant Mice

To determine whether the histological organization of the nervous system, including myelination, is affected in the *NCP1* mutant mice, we examined various regions of the CNS and PNS by light and electron microscopy (EM). Light microscopy did not demonstrate any obvious abnormalities in the histological organization or the extent of myelination. Figure 3A shows representative low-power micrographs of toluidine blue-stained sections of sciatic nerve and the ventral horn of the spinal cord. The numbers of myelinated fibers were indistinguishable between mutant and wild-type littermates. In addition, morphometric analysis of myelinated fibers in the PNS

Table 1. Morphometric Analysis of Myelinated Fibers in Sciatic Nerves of *NCP1* Mutant Mice

Parameter	+/+	−/−	p
Fiber diameter	3.44 ± 0.06	3.65 ± 0.05	NS
Axon diameter	2.00 ± 0.03	2.02 ± 0.03	NS
Myelin thickness	0.72 ± 0.02	0.81 ± 0.02	NS
g value	0.60 ± 0.003	0.57 ± 0.003	NS

Myelinated fibers from the sciatic nerves of three litter-matched pairs of P44–P45 +/+ and −/− mice were analyzed (one pair from each of three litters). A total of 507 and 570 fibers were measured from the +/+ and −/− animals, respectively. Diameter and thickness are presented in micrometers. Mean values ± SEM for all fibers are shown for each parameter. Measurements were analyzed statistically by paired t tests. NS indicates that the measured parameters for the +/+ and −/− mice (paired by litter) were not significantly different ($p > 0.05$).

showed no significant differences in axon and nerve fiber diameters, myelin thickness, or the g value (ratio of axon to fiber diameter) between *NCP1* and wild-type mice (Table 1). Two of the *NCP1* sciatic nerves had slightly thicker myelin (an average of ~0.14 μm thicker) compared to that of their wild-type littermates ($p < 0.0007$); the third pair were of comparable thickness. These results are consistent with an apparent increase in the thickness of some myelinated fibers in *NCP1* mutant mice and suggest that lack of NCP1 may be associated with mild hypermyelination.

To assess whether loss of NCP1 affected myelin composition, the levels of proteins expressed in compact myelin in the CNS were analyzed by Western blotting (Figure 3B). Expression of two components of compact myelin, proteolipid protein (PLP), and myelin basic protein (MBP) was unchanged in heterozygous and homozygous mutant mice. Expression of contactin, a protein that is complexed with NCP1 in the paranodal junctions (Rios et al., 2000), was also examined and found to be comparable to that of wild-type littermates (Figure 3B). Taken together with the histological analyses, these results indicate that loss of NCP1 does not affect compact myelin formation.

NCP1 is Required for Formation of Paranodal Junctions

Since NCP1 is localized to paranodal junctions, we examined the ultrastructure of this region in the CNS and PNS (Figure 3C). As shown in Figure 3Ca, paranodal loops are arrayed sequentially and in close apposition to the axonal membrane in the CNS of wild-type mice. Between the loops and axon, periodic densities corresponding to the septate-like transverse bands are readily apparent (Figure 3Ca, black arrowheads). In contrast, in the CNS of animals lacking NCP1, the paranodal and nodal morphology is frequently grossly perturbed (Figures 3Cb, 3Cc, 3Ce, and 3Cf). A consistent abnormality is the absence of the regular array of transverse bands between paranodal loops and the axon (Figures 3Ce and 3Cf). Occasionally, irregular densities were present between the glial loops and the axon (Figure 3Ce), suggesting that some residual junctional components may persist. The most striking paranodal abnormality consists of "everted" loops, i.e., paranodal loops that face away from, instead of toward, the axonal membrane (labeled el, Figure 3Cb and shown at higher magnification in Figure 3Cc). Everted loops are rarely observed at paranodes of wild-type spinal cords but are very frequent in the CNS of animals that lack NCP1. In other sites, the loops are severely disorganized in the paranodal region (Figure 3Cb, arrow).

Other striking abnormalities include occlusion of the node of Ranvier by paranodal loops from one myelin segment that override those from the opposite side, thereby creating a "pseudonode". In the example shown in Figure 3Cf, paranodal loops from the myelin segment on the right (labeled ol) override everted loops (labeled el) of the myelin segment on the left. Separation of the paranodal loops and the axon is increased in many cases (two examples are indicated with asterisks, Figure 3Cf). Similarly, the usual "scalloping" of the axolemma by the apposed paranodal loops is frequently reduced or absent. Additional defects included astrocytic processes that are interposed between the paranodal loops and the axon and the presence of Schmidt-Lanterman-like incisures in the myelin sheaths of the spinal cord (data not shown); these incisures are normally rare in CNS myelin.

As shown in Figures 3Cd and 3Cg, the organization of the paranodal loops is better preserved in the peripheral nerves. However, the characteristic transverse bands are consistently absent. In addition, the spacing between the paranodal loops and the axolemma is often abnormally wide (Figure 3Cd and inset in 3Cg), and the normal indentation of the axolemma by the paranodal loops is often absent. Occasionally, Schwann cell microvilli, which emerge from the outer collar of cytoplasm and normally project perpendicular to and contact the node of Ranvier (Raine, 1982), extend longitudinally into the periaxonal space (indicated by the brackets in Figure 3Cg). Comparable abnormalities are not observed in wild-type mice.

As a complement to the ultrastructural studies, we examined the organization of CNS nodal and paranodal regions by freeze-fracture analysis. Wild-type spinal cords show a high concentration of intramembranous particles in the node of Ranvier (Figures 4A and AE) that are believed to correspond to the voltage-gated Na^+ channels (Rosenbluth, 1995). The adjacent axon membrane exhibits successive transverse indentations that are characteristic of normal paranodes (demarcated by the white arrowheads in Figure 4A). In contrast, such indentations of the axon were not seen in any of the *NCP1* mutant mice (data not shown). A few membranes consistent with the nodal axolemmal E-face were observed. One example, shown in Figure 4B, arises from a transversely cut axon partially surrounded by paranodal loops (labeled 1, 2, and 3). Interestingly, the nodal particle density in this example is reduced (~700/μm^2) compared to that of wild-type nodes (1200/μm^2 in Figure 4A), suggesting that there is a lower density of Na^+ channels at the nodes of *NCP1* mutant mice. We also observed numerous examples of sequential arrays of narrow elongated profiles in the *NCP1* mutant spinal cord (Figure 4C, labeled a–g). These profiles correspond to the everted paranodal loops observed by EM (Figures 3Cb and 3Cc). These glial loops appose multiple layers of membranes that probably represent underlying my-

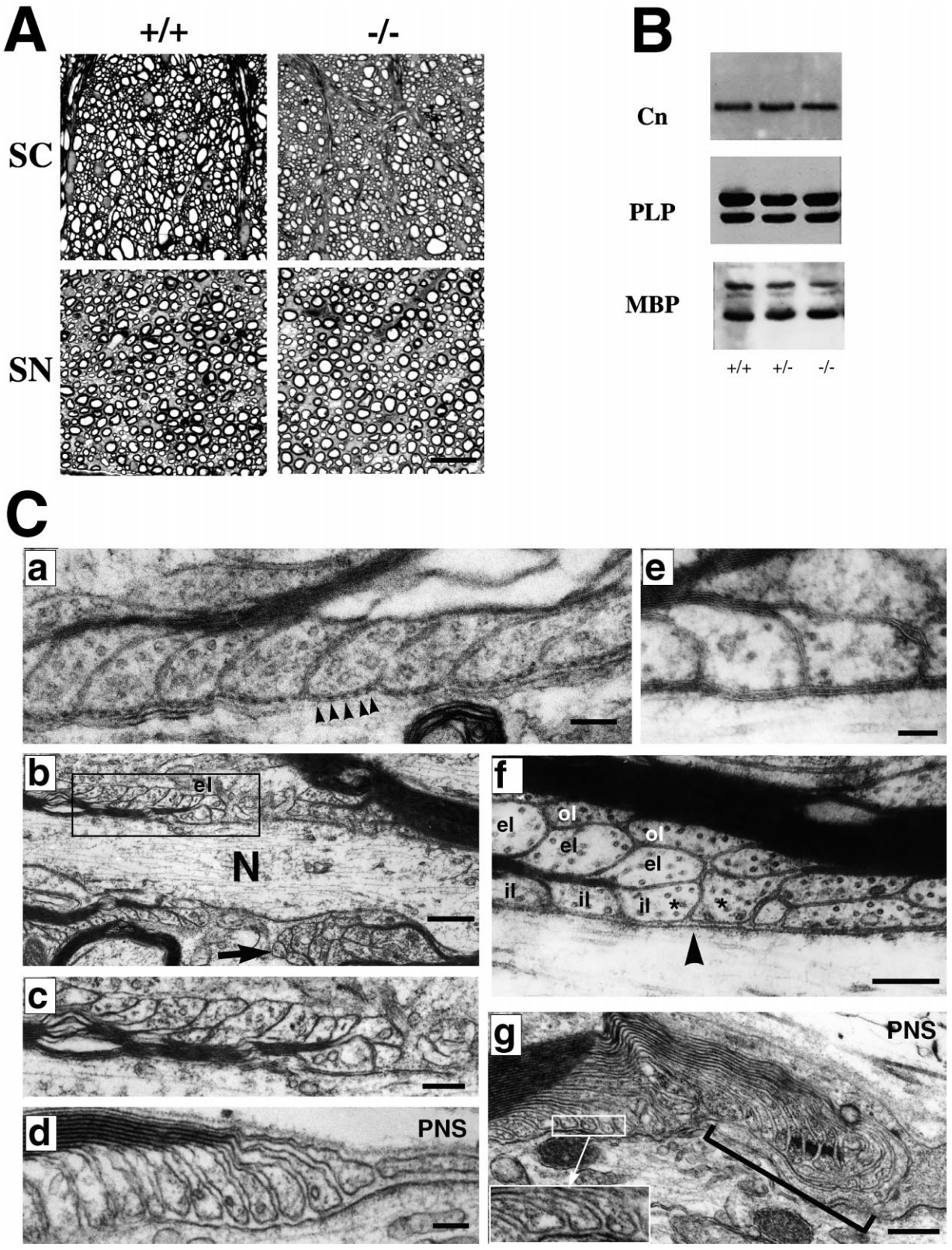

Figure 3. Myelin and Paranodal Morphology in Wild-Type and *NCP1* Mutant Mice

(A) Histologic analysis of myelination. Photomicrographs of toluidine blue sections through the ventral regions of the spinal cord (SC) and a portion of the sciatic nerves (SN) of wild-type (+/+) and *NCP1* mutant (−/−) mice are shown. Spinal cord sections were from ~P100 mice and sciatic nerve sections were from ~P24 mice. Myelinated axons cut in cross-section have pale axoplasm surrounded by dense compact myelin. Axon diameter and myelin sheath thickness are generally comparable to those in wild-type nerve. Bar, 20 μm.

elin lamellae (Figure 4C, indicated with asterisks). Taken together, these ultrastructural studies demonstrate that NCP1 plays a critical role in the normal organization and apposition of the paranodal loops to the axolemma and in the formation of the paranodal junctions.

Altered Distribution of Junctional Components in *NCP1* Mutant Mice

Our ultrastructural studies showed that the septate-like paranodal junctions are lacking in the absence of NCP1. We therefore examined the distribution of other proteins localized to this region. Contactin (Cn) normally forms a *cis* complex with NCP1 (Peles et al., 1997; Rios et al., 2000) on the axon in the paranodes of both the PNS and CNS (Figures 5A and 5I); it is also present at nodes of Ranvier in the CNS (Figure 5G; Rios et al., 2000). In *NCP1* mutant mice, contactin is not detectable in either the nodes or the paranodes of sciatic nerve fibers (Figure 5B). In contrast, contactin expression remains robust in mutant optic nerves but its distribution is altered. In wild-type optic nerves, much of contactin is confined to paranodal regions and low levels of protein are present in the nodal region (Figure 5G). In mutant optic nerves, contactin localization is more diffuse and higher levels of this protein are observed in the nodes than in the paranodes (Figures 5H and 5J, arrowheads). These data indicate that NCP1 is required for the proper localization of contactin to the paranodal domain.

The failure to detect contactin in sciatic nerves may result from a diffuse distribution along the axon that is below the limits of detection or the loss of the protein altogether. To distinguish these possibilities, we performed Western blot analysis of the expression of contactin in peripheral nerves. We found that both the large and small molecular weight isoforms of contactin are present in wild-type sciatic nerves. These correspond to free (e.g., non-NCP1-associated) and NCP1-associated forms, respectively (Rios et al., 2000). However, only the higher molecular weight isoform is detectable in the mutant peripheral nerves (data not shown). These results suggest that loss of NCP1 does not affect the free isoform of contactin, which is likely to be predominately expressed by nonmyelinated axons in the peripheral nerve (Rios et al., 2000).

Neurofascin is another protein localized to nodes and paranodes. Two neurofascin isoforms have been described: a 155 kDa isoform expressed by myelinating glia in paranodes (Davis et al., 1996; Tait et al., 2000) and a 186 kDa axonal isoform localized to nodes of Ranvier. The 186 kDa isoform is thought to be part of a complex that contains ankyrin and Na^+ channels (Bennett and Lambert, 1999). To determine whether the distribution of neurofascin was affected in *NCP1* mutants, we stained peripheral nerves with a polyclonal antibody that recognizes both isoforms of neurofascin. In wild-type peripheral nerves, neurofascin is present in both nodes and paranodes (Figure 5C, red inset). In contrast, in the absence of NCP1, neurofascin is enriched in nodes but reduced in paranodes (Figure 5D, red inset). Taken together, these data demonstrate that absence of NCP1 is associated with a loss of paranodal components, indicating that it plays an important role in the molecular organization of these junctions.

Ion Channel Distribution in the Absence of NCP1

A hallmark of myelinated axons is the localization of ion channels within discrete domains. Na^+ channels are concentrated at the nodes, whereas K^+ channels are largely restricted to the juxtaparanodes and to those regions of the internode that appose the noncompacted myelin membranes, e.g., the Schmidt-Lanterman incisures and the internal mesaxon (Peles and Salzer, 2000). To determine whether the defects at paranodal junctions in the mutant mice affect the distribution of these channels, we performed immunofluorescence staining of sciatic and optic nerves (Figure 6). In wild-type and mutant mice, Na^+ channels (green) are largely confined to the nodes of Ranvier. The distribution of the Na^+ channels is wider and more diffuse at the nodes of mutant mice, particularly in the optic nerve (Figure 6, ON). In contrast, the distribution of the K^+ channels (red) differs markedly between wild-type and *NCP1* mutant mice. In wild-type nerves, K^+ channels are completely separated from the Na^+ channels by the paranodes. In the mutant mice, K^+ channels are mislocalized to the paranodal region, immediately adjacent to and, in some cases, slightly overlapping with Na^+ channels (areas of overlap appear as yellow in the merged images). K^+ channel staining remained robust in the internodal axolemma of mutant mice. Interestingly, there is an increase in the number of stripes of K^+ channels along the axon. These stripes are apposed to the Schmidt-Lanterman clefts as confirmed by double staining with myelin-associated glycoprotein (MAG) antibody, a marker of these incisures

(B) Western blot analysis of myelin related proteins. Western blots of total brain extracts from wild-type (+/+), heterozygous (+/−), and *NCP1* mutants (−/−) were probed with antibodies to contactin (Cn), proteolipid protein (PLP), and myelin basic protein (MBP). No significant change in expression was observed.

(C) Perturbation of the paranodal organization of *NCP1* mutant mice. Electron micrographs through the paranodal region of wild-type (a) and *NCP1* mutant mice (b–g) are shown; panels (a)–(c), (e), and (f) are from the CNS (a, e and f, spinal cord; b and c, cerebellum), (d) and (g) are from the PNS (sciatic nerve). (Ca) shows wild-type spinal cord with paranodal loops tightly apposed to and indenting the axon, the characteristic transverse bands are also apparent (arrowheads). Bar, 0.1 μm. (Cb) shows mutant spinal cord with everted paranodal loops (boxed area, el); the node of Ranvier (N) is visible and disorganized paranodal loops are present to its right (arrow). Bar, 0.5 μm. (Cc) is a higher magnification of the everted loops in (Cb). Bar, 0.25 μm. (Ce) demonstrates closely apposed paranodal loops in the mutant spinal cord that display electron dense intramembranous material but lack transverse bands. Bar, 0.1 μm. (Cf) shows paranodal loops from one myelin segment that override loops from another segment thereby forming a "pseudonode" (arrowhead). Note the inwardly facing (il) and everted loops (el) of a myelin segment on the left and overriding loops (ol) from a myelin segment on the right; the entire complex is covered by thick compact myelin. Loops marked with an asterisk are unusually widely spaced from the axolemma. Bar, 0.25 μm. In the PNS (d and g), the paranodal loops face the axon but fail to closely appose or form transverse bands with the axolemma (Cd and Cg, inset); a Schwann cell microvillar process (indicated with brackets) is interposed between the terminal loops and the axon (Cg). Bars: 0.1 μm (d), 0.25 μm (g).

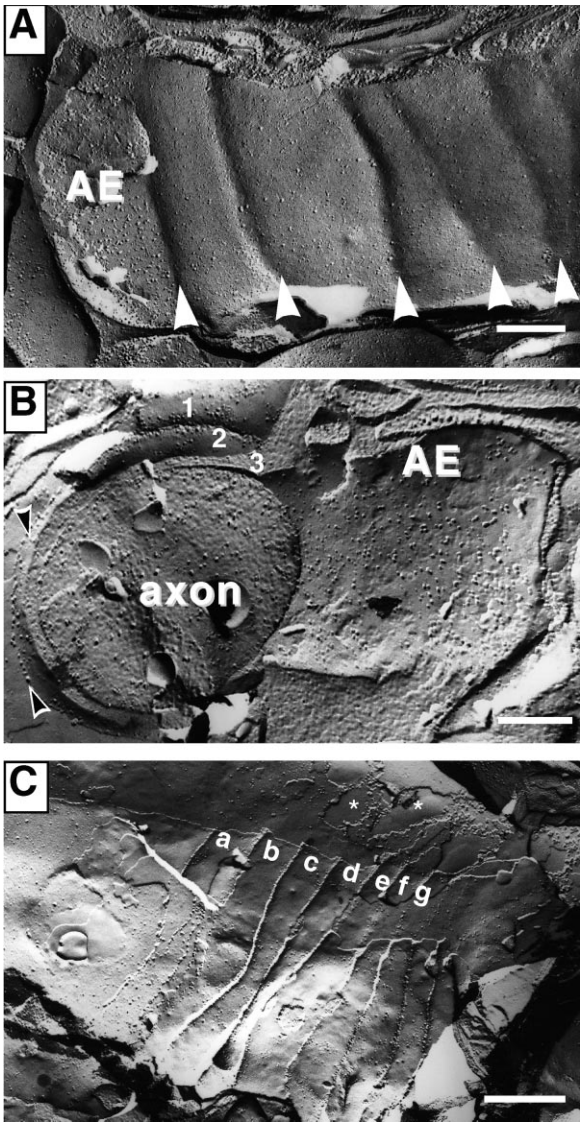

Figure 4. Freeze Fracture Analysis of Nodal and Paranodal Regions

(A) Freeze-fracture replicas from wild-type spinal cord show the E-face of the axolemma with indentations imposed on the axon by paranodal loops (behind the plane of the picture). A short section of nodal axolemma (AE), on the left, contains intramembrane particles at a density of ~1200/μm^2 that are sharply demarcated by the first indentation. Bar, 0.25 μm.

(B) A freeze-fracture replica from an *NCP1* mutant spinal cord shows a transversely cut axon on the left, which is partially surrounded by three paranodal loops (numbered 1, 2, and 3). The E-face of the axolemma (AE) extending from the center toward left displays node-like intramembrane particles at a density of ~700/μm^2. Tight junctions which are present between the paranodal loops are also visible (black arrowheads). Bar, 0.25 μm.

(C) A freeze-fracture replica from an *NCP1* mutant spinal cord shows the E-face of everted glial loops (a–g) that aberrantly adjoin multiple layers of compact myelin (several of which are indicated with asterisks). Bar, 0.5 μm.

(data not shown). Hence, these data indicate that paranodal junctions are required for the segregation of Na^+ and K^+ channels into distinct, nonoverlapping domains.

Nerve Conduction Velocity Is Markedly Reduced in *NCP1* Mutant Mice

To determine whether the absence of the paranodal junctions and/or the altered distribution of ion channels affected the electrophysiological properties of the peripheral nerve, we performed field potential recordings on sciatic nerves. From the measured compound action potentials (CAP), we calculated population conduction velocities (CV) (Figure 7; Table 2). Low-frequency stimulation of sciatic nerves at maximal intensity yielded a CV of 25.01 $\pm$ 1.22 m/s for wild-type nerves and 14.78 $\pm$ 0.80 m/s for *NCP1* mutant nerves, a 41% reduction. Low-frequency stimulation at half-maximal intensity yielded a CV of 23.50 $\pm$ 0.92 m/s for wild-type nerves and 13.63 $\pm$ 0.82 m/s for mutant nerves, a 42% reduction. CAP peak-to-peak amplitudes were also significantly reduced (45% at both maximal and half-maximal stimulation) in mutant mice. The reductions in CV and CAP peak-to-peak amplitude were statistically significant ($p < 0.001$) and were consistently observed from P47 to P107.

In addition to these changes, we noted a difference in CAP waveforms between wild-type and *NCP1* mutant nerves. Wild-type CAPs demonstrated a smooth waveform while mutant CAPs showed, in addition, a delayed deflection (Figure 7, arrowheads). The mechanism(s) responsible for this change is not yet known but may include conduction block in the mutants of a subpopulation of fibers or changes in the conduction parameters of mutant myelinated fibers. We also observed a trend toward a frequency-dependent increase in CAP latency and a decrease in amplitude with prolonged high-frequency stimulation, although these findings were not statistically significant (data not shown). Thus, the electrophysiological analyses indicate that the axon-glial interactions mediated by NCP1 at the paranodes are crucial for normal saltatory conduction.

Discussion

The ultrastructure of the paranodal region was first described over four decades ago (Robertson, 1957; Andres, 1965; Bargmann and Lindner, 1964), but its molecular composition remained elusive until the identification of NCP1 as a major junctional component (Einheber et al., 1997; Menegoz et al., 1997). Our data show that NCP1 is an essential component of the paranodal junctions. The *NCP1* mutant mice therefore provide a unique model to dissect the function of paranodal junctions in myelinated axons.

Phenotypic Abnormalities of *NCP1* Mutant Mice

In the absence of NCP1, mice exhibit tremors, paresis, and ataxia. We believe that these neurologic defects reflect the function of NCP1 in the nervous system since we did not observe its expression in non-neuronal tissues (e.g., lung, heart, kidney, stomach, intestine, pancreas, and testes) by Western blotting analysis (data not shown). While these *NCP1* mutant mice also lack *CCR10* (Figure 1B), neither CCR10 (Jarmin et al., 2000, Homey et al., 2000) nor its ligand (Wang et al., 2000) are expressed in the nervous system. Importantly, *CCR10* mutant mice were recently generated and do not exhibit any neurologic phenotype (C. Gerard, personal commu-

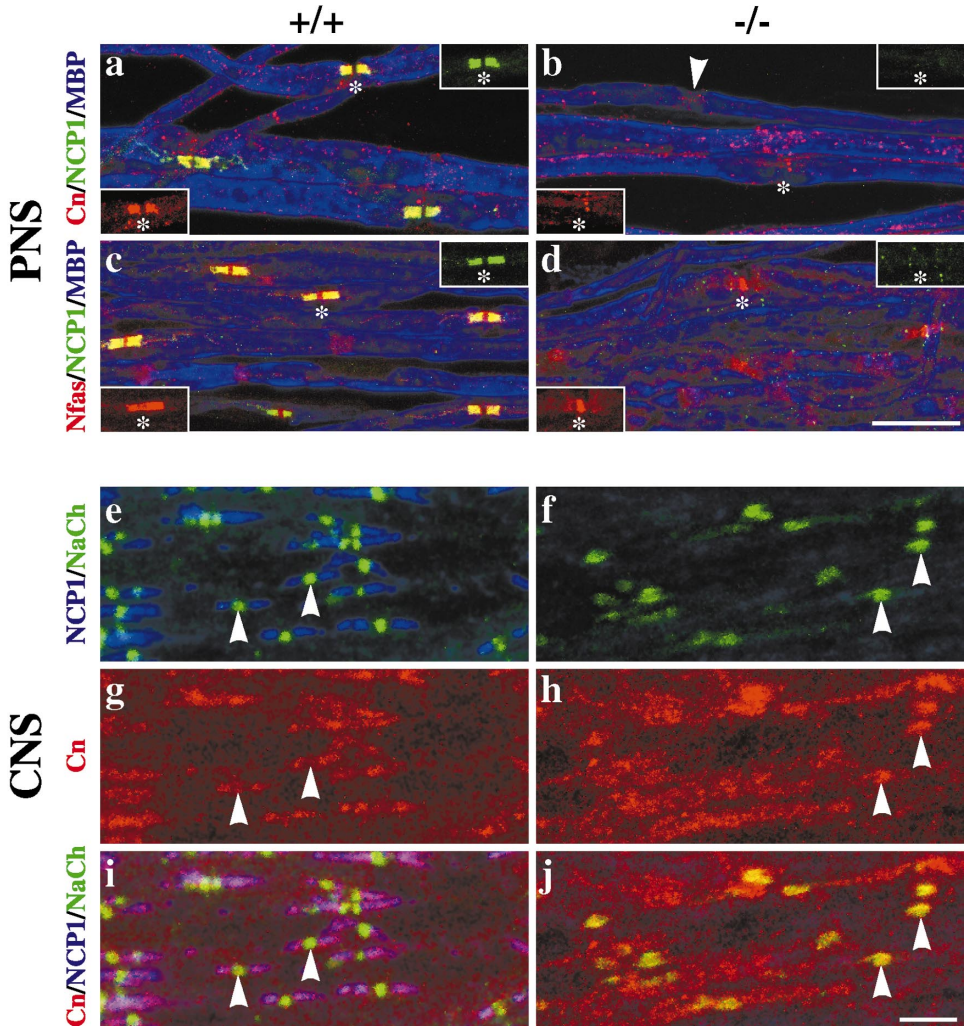

Figure 5. Expression of Paranodal Markers in Sciatic and Optic Nerves

Teased sciatic nerves (PNS, A–D) and cryosections of optic nerves (CNS, E–J) from wild-type (+/+) and *NCP1* mutant (−/−) mice were stained for paranodal markers. Sciatic nerves were stained with NCP1 and MBP, and either contactin (Cn, A and B) or neurofascin (Nfas, C and D). The insets highlight a single node, indicated with an asterisk. In the wild-type nerves, NCP1 colocalizes with Cn in the paranodes; Nfas is present in both the node and paranodes. In the mutant nerve, NCP1 and Cn are not detectable in the paranodes and Nfas is largely present at the node. A second node is shown in (B) (white arrowhead). Bar, 20 μm.

Optic nerves were stained for NCP1, Cn, and Na^+ channels (NaCh); several nodes are highlighted by the white arrowheads. In the wild-type nerves (E, G, and I), Na^+ channels at the nodes are flanked by NCP1 and Cn in the paranodal regions; Cn is also present at low levels at the node (G, arrowheads). In mutant nerves (F, H, and J), much of the Cn colocalizes with NaCh in the nodes (J, yellow in the merged images), whereas low levels are present in the paranodes. Bar, 5 μm.

nication). Thus, loss of *CCR10* is unlikely to contribute to the observed neurologic phenotype in the mutant mice. While we have focused our efforts on the paranodal junctions and the organization of myelinated fibers, NCP1 is also expressed by nonmyelinated axons and in the central gray matter (Einheber et al., 1997; Menegoz et al., 1997). Therefore, the neurologic abnormalities may be due to paranodal and extrajunctional defects.

The neurologic defects of these mice resemble those of the recently described contactin mutant mice (Berglund et al., 1999). As contactin is also localized to the paranodes (Rios et al., 2000) and is required for the cell surface expression of NCP1 (Faivre-Sarrailh et al., 2000), it will be of interest to determine the organization of the paranodal region in these mutant mice. Contactin mutant mice are ataxic and have striking defects in cerebellar development, reflecting its expression by several types of cerebellar neurons and its role in mediating neurite outgrowth and neuronal interactions (Faivre-Sarrailh and Rougon, 1997). NCP1 has been suggested to function as a coreceptor for contactin and is highly expressed within the cerebellum (Peles et al., 1997; G.P.G.-F. and M.B., unpublished data). Although the cerebellar development of *NCP1* mutant mice has not been examined, the ataxia, wide-based gait, and tremor of these mice may reflect defects of cerebellar development rather than abnormalities of the paranodal region per se. Contactin mutant mice are likely to exhibit more

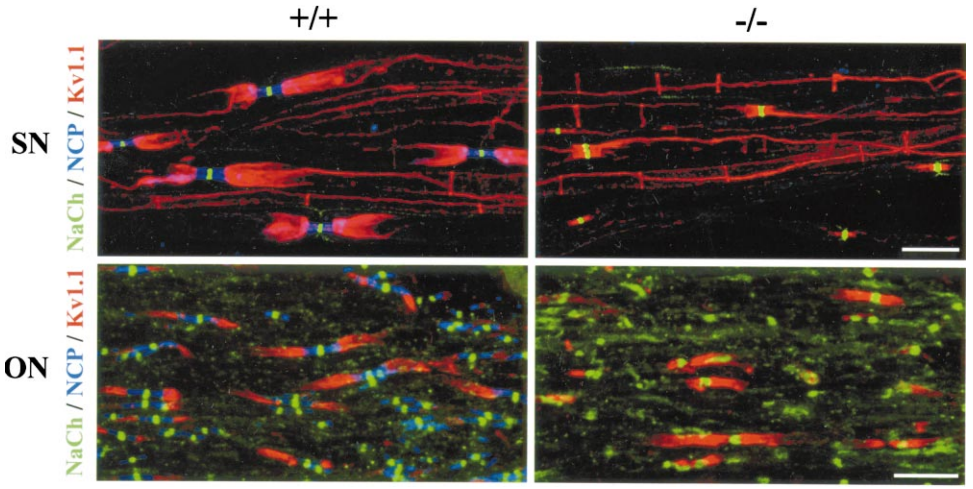

Figure 6. Voltage-Gated Channel Distribution Is Perturbed in *NCP1* Mutant Mice

Teased sciatic nerves (SN) and cryosections of optic nerves (ON) from wild-type (+/+) and *NCP1* mutant (-/-) mice were stained with antibodies to ion channels. In the wild-type sciatic and optic nerves, the Na^+ channels (NaCh, green) and K^+ channels (Kv 1.1, red) are completely separated by NCP1 (NCP, blue) in the paranodes. In the mutant nerves, K^+ channels are aberrantly localized to the paranodes and overlap slightly with Na^+ channels (regions of overlap are yellow). In the PNS, there is also prominent K^+ channel staining in vertical stripes that appose Schmidt Lanterman incisures. Bars, 20 μm (SN); 10 μm (ON).

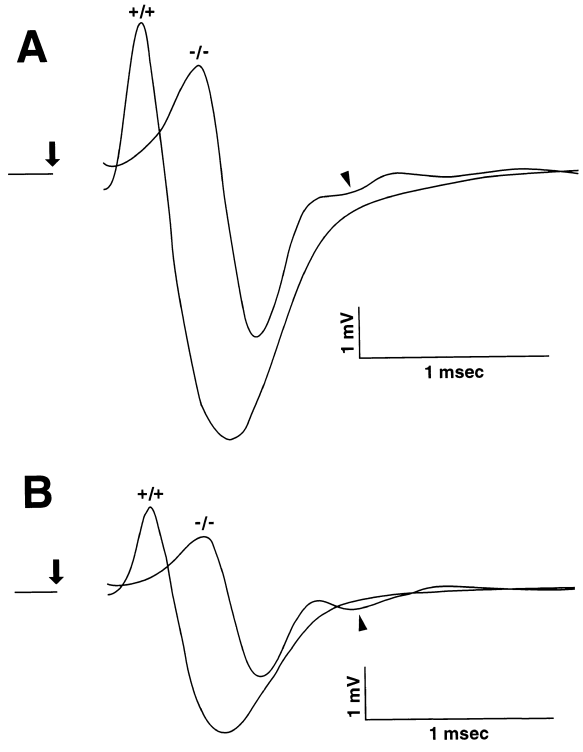

Figure 7. Electrophysiological Analysis of *NCP1* Mutant Mice

(A) Low-frequency (0.2 Hz) compound action potentials (CAP) of sciatic nerves demonstrate a difference in the CAP waveforms between wild-type (+/+) and *NCP1* mutant (−/−) mice stimulated at maximal intensity. Note that CAPs from the mutant nerves exhibit a markedly reduced peak-to-peak amplitude and delayed time of onset compared to wild-type nerves. Mutant nerves also show a delayed deflection (arrowhead). Arrow indicates time of stimulation. (B) Low-frequency (0.2 Hz) CAP stimulated at 1/2 maximal intensity also demonstrate a difference between the waveforms of wild-type and mutant mice; the delayed deflection is indicated (arrowhead).

widespread defects than *NCP1* mutant mice in view of the extrajunctional expression of this protein at central nodes of Ranvier, by oligodendrocytes, and, potentially, specific neurons.

Abnormal Axon-Glial Interactions at the Nodes and Paranodes of *NCP1* Mutant Mice

A major defect of the mutant mice is the absence of transverse bands, the hallmark of the paranodal junctions. These findings provide formal evidence that NCP1 is a key axonal component of these junctions, consistent with its striking localization to these junctions (Einheber et al., 1997; Menegoz et al., 1997). In addition, the close apposition and indentation of the axon by the paranodal loops was frequently absent and, in the most severe cases, the paranodal loops were detached from the axon (Figure 3Cd). These results indicate that NCP1 is required to stabilize the adhesion of these loops to the

Table 2. Electrophysiologic Analysis of Sciatic Nerves

Maximal Stimulation				
	PkAmp (mV)	Latency (ms)	CV (m/s)	n
+/+	6.49 ± 0.57	0.41 ± 0.02	25.01 ± 1.22	10
−/−	3.60 ± 0.24	0.62 ± 0.03	14.78 ± 0.80	11
1/2 Maximal Stimulation				
	PkAmp (mV)	Latency (ms)	CV (m/s)	n
+/+	3.37 ± 0.27	0.43 ± 0.02	23.50 ± 0.92	10
−/−	1.87 ± 0.15	0.66 ± 0.04	13.63 ± 0.82	9

This table shows results of low-frequency stimulation of sciatic nerves at empirically determined maximal and half-maximal intensities. Sciatic nerves from the *NCP1* mutant mice showed significantly decreased population conduction velocities (CV), evidenced as increased compound action potential (CAP) latencies. In addition, they exhibited decreased CAP peak-to-peak amplitudes (PkAmp) when compared to wild-type nerves ($p \ll 0.001$ for both measurements). Measurements are expressed as mean ± SEM.

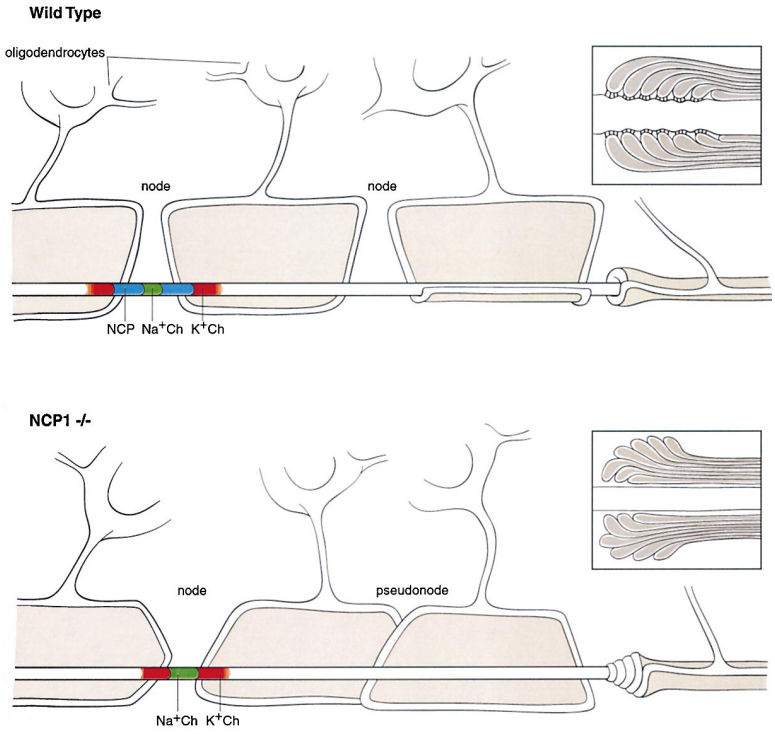

Figure 8. Summary of the Nodal and Paranodal Abnormalities in the *NCP1* Mutant Mice

Schematic illustration of myelin sheaths elaborated by oligodendrocytes associated with axons in wild-type and *NCP1* mutant mice. In wild-type mice, the myelin sheaths have a trapezoidal shape when unrolled; the sheaths are wider in their proximal region, which forms the outer myelin lamellae. In contrast, in many of the myelin segments of the *NCP1* mutant mice, the trapezoidal shape is inverted and the distal region is wider. Corresponding insets show the normal organization of the paranodal junctions in the wild-type mice and the everted arrangement of paranodal loops in the knockout mice. Other knockout abnormalities in the *NCP1* mutants include segments that are wider in the middle of the sheath, which would give rise to a double row of paranodal loops, or adjacent segments that overlap in the presumptive nodal region resulting in "occluded pseudonodes". The channel distribution in wild-type and mutant mice is also shown, including the mislocalization of the K^+ channels in the *NCP1* mutant mice.

axon, either directly or in combination with other junctional components. Interestingly, the paranodal loops occasionally retain a close association with the axon and, in these cases, some intramembranous density is apparent by EM (see Figure 3Ce). These findings suggest that other components of the junctions, yet to be identified, may be able to promote axon attachment in the absence of NCP1. Alternatively, Caspr2, which shares high homology to NCP1 in its ectodomain (Poliak et al., 1999) and which is mislocalized from the juxtaparanodes into the paranodal region of *NCP1* mutant mice (data not shown), may contribute to this adhesion.

In the CNS, the morphologic organization of the paranodal region is often grossly perturbed—most strikingly represented by the eversion of the glial loops (Figures 3Cb, 3Cc, and 3Cf). Defective attachment of the paranodal loops to the axon in these mice seems likely to account for this anomalous morphologic organization. The myelin sheath is elaborated by circumferential growth of the inner turn of the glial cell membrane that spirals around the axon (Bunge et al., 1989). In the *NCP1* mutant mice, frequently only the paranodal loops of the innermost myelin turns remained attached to the axon, whereas the lateral loops of the outermost turns were often unattached, everted, and displaced medially (Figure 8, bottom). The latter findings indicate that the normal trapezoidal organization of the myelin sheath is reversed (illustrated schematically in Figure 8). It is not known when the loops detach: potentially the inner turn of the myelin sheath may displace existing glial contacts with the axon as it spirals around the axon, or alternatively, the loops may detach after myelin sheaths have already formed. Other abnormalities, including loops from a single myelin sheath that appose each other and myelin segments that overlap, also suggest defective glial attachment. Several of these morphologic abnormalities are illustrated in Figure 8. Interestingly, these gross abnormalities were only observed in the CNS. Potentially, the presence of a well-formed basal lamina and/or the Schwann cell microvilli which project to the node (Melendez-Vasquez et al., 2001), both of which are unique features of PNS myelin, may stabilize the paranodal loop organization sufficiently to prevent these abnormalities. As the amount and organization of compact myelin was not affected in the mutant mice, radial growth of the myelin sheath does not require NCP1.

NCP1 Mutant Mice Are Deficient in Junctional Components

Based on immunofluorescence staining of peripheral nerves, two other components of the paranodal junctions, contactin and neurofascin, which are expressed by neurons and Schwann cells, respectively (Rios et al., 2000; Tait et al., 2000), are undetectable or substantially reduced in the paranodal region. Initial immunoblotting studies of sciatic nerve extracts show that a lower molecular weight isoform of contactin that specifically associates with NCP1 (Rios et al., 2000) is undetectable and that the 155 kDa isoform of neurofascin is significantly reduced (data not shown). Thus, there is a global deficiency of the known paranodal components in the *NCP1* mutant mice. Whether the loss of these components reflects the failure of the paranodal loops to attach to axons properly in the absence of NCP1 or, alternatively, that these components are not properly targeted or are unstable in the absence of NCP1, is not yet known. However, loss of contactin and neurofascin is likely to further contribute to the defects of glial loop adhesion.

In the CNS, contactin is expressed at comparable levels in wild-type and *NCP1* mutant mice (Figure 3B)

but its localization is perturbed. Specifically, staining of contactin in the paranodes is reduced whereas that in the nodes of Ranvier is increased and appears diffuse (Figure 5). These findings suggest that in the absence of NCP1, contactin redistributes from the paranodes to the nodes and provide further evidence that NCP1 is required for the appropriate targeting of contactin to the paranodes (Rios et al., 2000). The normal expression levels of contactin seen by Western blotting may reflect a non-NCP1-interacting pool of this protein in oligodendrocytes (Einheber et al., 1997; Koch et al., 1997) and at nodes of Ranvier in the CNS. These findings may also indicate that neuronal expression of contactin in extrajunctional sites is not dependent on NCP1.

Paranodal Junctions and Domain Organization in Myelinated Axons

A striking finding of this study is that the delineation between channel domains requires NCP1 and the transverse bands. In their absence, the delayed rectifier K^+ channels are displaced into the paranodes adjacent to the node. The data also indicate that Na^+ and K^+ channels still cluster in the absence of these junctions. This is consistent with previous studies demonstrating that nodal clustering occurs prior to mature paranodal junction formation in the developing PNS (Melendez-Vasquez et al., 2001) and in the *CGT* mutant mice, which fail to form normal junctions (Dupree et al., 1999). It is of note that Na^+ and K^+ channel domains remain largely segregated, suggesting that even in the absence of the transverse bands, unique molecular interactions, possibly involving distinct scaffolding proteins (Peles and Salzer, 2000), maintain the separation of these channel domains. K^+ channels associate with the closely related Caspr2 protein (Poliak et al., 1999), which is also mislocalized to the paranodes (data not shown).

Our data also show that CAP peak-to-peak amplitudes and population nerve conduction velocities (CV) are markedly reduced in the peripheral nerves of *NCP1* mutant mice. These findings are most readily explained by changes in the properties of fast-conducting myelinated fibers, in particular, a decrease in the number of conducting nerve fibers due to conduction block and slower propagation in the remaining fibers. Disrupted paranodal junctions may explain both changes. A slower CV may result from current leakage through the disrupted paranodal junctions into the periaxonal space, which would be expected to increase the capacitance of the axonal membrane, delay its charging, and slow action potential propagation. In addition, these fibers may experience conduction block due to this shift toward a more electrotonic mode of conduction without a compensatory change in internodal Na^+ channel expression. These changes do not appear to reflect an increase in the proportion of slower conducting, small diameter nerve fibers based on morphometric analysis (Table 1). It will be of interest to determine whether the electrophysiological alterations are even more pronounced in the CNS, given the more severe perturbations of the paranodal organization observed by EM (Figure 3).

The paranodal defects of the *NCP1* mutant mice strikingly mirror those in the *CGT* mutant mice (Coetzee et al., 1996). Common features of both mutant mice include the absence of transverse bands, everted loops, and other paranodal abnormalities in the CNS, an increase in the number of Schmidt-Lanterman incisures in CNS myelin, and the relatively normal morphology of the paranodal region in the PNS. These common findings are reflected in the loss of the delineation between the channel domains and a reduction in the nerve conduction velocity and amplitude in the PNS (Dupree et al., 1998). Our results, therefore, indicate that the defects in the K^+ channel distribution in the *CGT* mutant mice are likely to be secondary to the loss of the paranodal junctions rather than a more generalized effect on myelin. There are, however, differences between the *CGT* and *NCP1* mutant mice. In particular, we did not observe the extensive myelin splitting or vacuolar degeneration in the *NCP1* mutant mice that has been reported for the *CGT* mutants (Coetzee et al., 1996). This degeneration had been suggested to result from increased permeability resulting from the loss of junctional integrity and entrance of fluid into the periaxonal space (Dupree et al., 1998). As such degeneration is limited in the *NCP1* mutant mice, the vacuolar degeneration may instead reflect abnormalities in the glycolipid composition of the *CGT* mutant mice. In addition, the K^+ channels in the *CGT* mutant mice exhibit a more diffuse distribution within the internodes rather than the discrete paranodal distribution characteristic of the *NCP1* mutant mice (see Figure 6). These latter results suggest that the glial interactions that regulate the distribution of K^+ channels may be more globally affected in the *CGT* mutant mice than in the *NCP1* mutant mice.

The striking homology between these mutants provides further support for a role of Gal C and/or sulfatides in the formation of the paranodal region. An interesting possibility is that these glycolipids are themselves ligands for NCP1. Indeed, NCP1 is diffusely distributed throughout the internode in the *CGT* mutant mice, rather than confined to the paranodal region (Dupree et al., 1999). In addition, NCP1 contains a discoidin domain and laminin G domains that exhibit structural homology to lectins (Rudenko et al., 1999). Interestingly, laminin G domains bind several ligands including sulfatides (Talts et al., 1999). Alternatively, defects of these glycolipids may have generalized effects on the myelin sheath, including the composition or trafficking of glial junctional components.

Conserved Function of the NCP Family during Evolution

Septate junctions form between the ensheathing glial cells that surround the nerve bundles in *Drosophila* and are essential for establishment of the blood-nerve barrier (Bellen et al., 1998). We have previously shown that the *Drosophila* NRX IV protein localizes to and is required for the formation of the ladder-like septae characteristic of these junctions (Baumgartner et al., 1996). In *nrx IV* mutants, these septae were absent, and another component of these junctions, Coracle, a band 4.1 homolog, was mislocalized (Baumgartner et al., 1996; Ward et al., 1998). The current studies demonstrate that the septate and paranodal junctions appear to serve conserved functions in maintaining the axonal milieu re-

quired for action potential propagation. However, the topology and localization of the proteins is clearly different. In *Drosophila*, NRX IV is expressed by and localized between glial cells. In mice and other vertebrates, NCP1 is expressed by neurons and localized between the axon and glial cells. Hence, even though there is functional conservation, significant changes in expression occurred during evolution.

In summary, we have demonstrated that NCP1 has a key role in the formation of the paranodal junctions and, thereby, in the delineation of the axonal domains of myelinated axons. Future studies focused on the identification of other components of these junctions, including the glial ligands for NCP1 and the cytoskeletal protein(s) with which it interacts, should clarify how these junctions assemble and the mechanisms by which they promote separation of distinct populations of voltage-gated ion channels.

Experimental Procedures

Antibodies

Sequences corresponding to the cytoplasmic region of *NCP1* were cloned into an expression vector, pET-28a(+) (Novagen). The recombinant protein was expressed in *E. coli* BL21(DE3), resolved by SDS-PAGE, and used to immunize guinea pigs as described in Bhat et al. (1996). Other antibodies used included rabbit polyclonal antibodies to contactin-Fc (Rios et al., 2000), to human contactin/F3 (J. Hemperly, Becton Dickinson), to neurofascin (P. Brophy, University of Edinburgh, Scotland), to PLP (D. Colman, Mount Sinai, New York), a chicken antibody to ankyrin$_G$ (S. Lambert, University of Massachusetts Medical Center), and mouse monoclonal antibodies to the α subunit of the voltage-gated Na^+ channel (J. Trimmer, SUNY, Stony Brook) and to MBP (SMI 94; Sternberger Monoclonals). The secondary antibodies conjugated to rhodamine, fluorescein, or Cy-5 were obtained from Jackson Laboratories.

Preparation of Teased Sciatic Nerves and Optic Nerve Sections

Sciatic nerves were removed from litter-matched wild-type and mutant mice and fixed in phosphate buffer saline (PBS) with 1% or 4% paraformaldehyde for 1.5 hr. The nerves were then stored in PBS at 4°C until teased. Using fine needles, the individual fibers of the sciatic nerve were teased while in ice-cold PBS. Teased sciatic nerve fibers (TSNs) were then mounted on glass slides and dried overnight at RT followed by treatment with acetone at −20°C for 20 min. The slides were washed with PBS several times before immunostaining; in some cases, slides were stored at −80°C until processed further. Optic nerves were dissected out and fixed in 1% paraformaldehyde in PBS for 1.5 hr. Nerves were stored in PBS, cryoprotected with 30% sucrose, and frozen in Tissue-Tek OCT with isopentane cooled in liquid nitrogen. The tissue was sectioned at 10 μm on a Leica CM1900 cryostat with a chamber temperature of −26°C and stage temperature of −28°C.

Immunofluorescence and Western Blot Analysis

Fixed tissue samples (TSNs and optic nerve sections) were permeabilized with acetone at −20°C, washed with dPBS, and blocked for 1 hr at room temperature in a blocking solution consisting of dPBS, 5% BSA, 1% normal donkey serum, and 0.2% Triton X-100 (Sigma Chemical). Primary antibodies diluted in blocking solution were added and left overnight in a humidifying chamber at 4°C. After washing several times with dPBS plus 0.2% Triton X-100, the tissue was incubated with corresponding secondary antibodies at a dilution of 1:100 in blocking solution for 1 hr at RT. For labeling with anti-contactin, tissue was incubated with anti-contactin alone overnight and stained with donkey anti-rabbit rhodamine, prior to incubation with anti-NCP1 and anti-sodium channel antibodies. The tissue was then washed several times with dPBS, washed once with water, and mounted in Citifluor (Ted Pella, Redding, CA). The tissue was examined by epifluorescence on a Zeiss LSM 510 confocal microscope.

Whole brain or sciatic nerve lysates were prepared in 25 mM Tris-HCl buffer, pH 7.4, containing 2% SDS, 95 mM NaCl, 10 mM EDTA, 0.2 mM sodium vanadate, 10 mM sodium pyrophosphate, 1 mM PMSF, 10 μg/ml aprotinin, and 20 μM leupeptin, boiled for 5 min, and centrifuged for 10 min. The lysates were quantitated and subjected to SDS gel electrophoresis, blotted onto nitrocellulose, probed with primary antibodies and developed using the SuperSignal chemiluminescent substrate (Pierce).

NCP1 Targeting Vector

A mouse 129Sv/Ev genomic library in λFIX II (Stratagene) was screened and overlapping genomic DNA phage clones were isolated to establish a contiguous map of the *NCP1* locus. The genomic DNA fragments containing the exonic sequences in the 5′ region of the gene were sequenced to determine the intron-exon structure. Based on the sequence information, a partial intron-exon structure of the *NCP1* locus was established that helped us design a targeting construct such that the 5′ end of the gene carrying the first 7 exons encoding the N-terminal 327 amino acids will be deleted. A *pgk-HPRT* resistance cassette was flanked by a 3.8 kb EcoRI-BamHI fragment (5′ homology) and a 4.5 kb EcoRI-SmaI fragment (3′ homology). Herpes simplex virus *thymidine kinase* (*hsv-tk*) was added to the 3′ end of the construct as a negative-selectable marker (for detailed map, see Figure 1B, construct #1). The linearized targeting vector was electroporated into AB2.2 embryonic stem (ES) cells (Sharan et al., 1997). This construct failed to produce any resistant ES clones. Another targeting vector was constructed in which a 2.9 kb BamHI-XhoI fragment served as the 5′ homology region and a 4.5 kb EcoRI-SmaI fragment served as the 3′ homology region disrupted by insertion of *pol II-neo* resistance cassette (Figure 1B, construct #2). The linearized targeting vector was electroporated as above and targeted ES clones were obtained. Standard cell culture and molecular biological procedures were used to confirm the targeting event in the *NCP1* locus.

Electron Microscopy and Freeze Fracture Analysis

Wild-type and mutant littermates (P21–P100) were anesthetized with pentobarbital and perfused through the heart with either 3% glutaraldehyde/2% paraformaldehyde in 0.1 M cacodylate buffer, pH 7.3 (fixative 1), or 4% paraformaldehyde/2.5% glutaraldehyde in 0.1 M phosphate buffer, pH 7.4 (fixative 2). Samples of spinal cord, optic nerve, cauda equina, trigeminal nerve, and sciatic nerve prepared with fixative 1 were rinsed and postfixed in osmic acid/ferricyanide in 0.1 M cacodylate buffer. They were rinsed, dehydrated in an ascending series of methanol solutions, and embedded in Araldite. One micron sections were stained with toluidine blue for light microscopy, and 0.1 μm sections were stained with potassium permanganate followed by uranyl acetate for ultrastructural examination. The brain, spinal cord, and sciatic nerves prepared with fixative 2 were postfixed in the same solution for an additional 18–24 hr at 4°C. Vibratome sections (40 μm) of the brain and spinal cord, and whole sciatic nerves were processed, embedded in Epon 812, and sectioned for electron microscopy as previously described (Einheber et al., 1997). Thin sections were examined with Philips 300, CM10, or CM 12 electron microscopes at 60 kV. Color light micrographs of toluidine blue stained sections were scanned and digitized or taken directly with a Nikon digital camera.

Morphometric analysis was performed on electron micrographs (8260× magnification) of random fields of sciatic nerves (prepared with fixative 2) that were cut in cross-section at the midthigh region. Nerves from three 44- to 45-day-old litter and sex-matched pairs of *NCP1* and wild-type mice were examined. Total fiber (myelin plus axon) and axonal areas of all profiles that were clearly cut in the transverse plane, as judged by fiber morphology and orientation of axonal microtubules, were determined using a computer drawing tablet and the Image 1.50 program (National Institutes of Health, Bethesda, MD). From these values, fiber and axonal diameters, which actually corresponded to the diameters of circles with the measured areas, and myelin thickness were arithmetically derived. The data were analyzed statistically using paired t tests.

For freeze-fracture analysis, aldehyde-fixed specimens were Vi-

bratomed at 50 μm. Sections were cryoprotected with glycerine, fractured in a Balzers 080 unit, and shadowed unidirectionally with platinum and carbon. Tissue was digested with bleach and the replicas mounted on copper grids. Electron microscopy and processing of micrographs was carried out as described above.

Electrophysiological Studies

Wild-type and *NCP1* mutant mice were anesthetized with isoflurane and sacrificed by decapitation. Sciatic nerves were then removed and maintained in Ringer's solution (124 mM NaCl; 3 mM KCl; 1 mM Na_2HPO_4; 26 mM $NaHCO_3$; 1.5 mM $MgSO_4$; 1.5 mM $CaCl_2$; and 10 mM dextrose) oxygenated with 95% O_2/5% CO_2 at RT. Microelectrodes were fabricated from borosilicate capillary glass with an internal filament (o.d. 1.5 mm, i.d. 0.86 mm; A-M Instruments) using a PE-2 micropipette puller (Narishige Scientific Instruments). Microelectrodes had an average tip diameter of 4 μm and were backfilled with 2 M KCl. The microelectrode was connected by means of an Ag/AgCl wire and HS-2 10× head stage to an Axoprobe-1A amplifier (Axon Instruments). Voltage outputs were monitored in real time on an oscilloscope and digitized with a Neurocorder (Neurodata Instruments) to videotape for offline data access. Computerization and automated analysis (peak and latency measurements) were done using pClamp 7 (Axon Instruments). Subsequent analysis and visualization were performed using Excel 98 (Microsoft). To measure compound action potentials, nerves were superfused with oxygenated Ringer's solution at 37°C ±1°C and stimulated orthodromically with a Teflon-insulated bipolar platinum-iridium electrode for 50 μs at currents empirically determined to elicit maximal and half-maximal CAP amplitudes. Response to low-frequency stimulation was assessed at 0.2 Hz, while response to high-frequency train stimulation was assessed at 10, 20, and 33 Hz. The animals varied in age from 47 to 107 days and generally included age- and sex-matched pairs, although neither the age nor sex of the animals appeared to influence the CAP properties. Statistical analysis of the nerve conduction velocities obtained was determined by Student's two-tailed unpaired t test.

Phenotypic Analysis of Mice

Weights were obtained daily up to P30, with data collected from 19 homozygous males, 44 heterozygous males, 24 wild-type males, 20 homozygous females, 30 heterozygous females, and 20 wild-type females; later time points correspond to fewer numbers of animals. To measure the motor activity, an open field test was performed at P21, P40, and P100 as described (Thullier et al., 1999). Briefly, animals were placed one at a time in standing position in the same middle square in a rectangular area 55 cm long by 30 cm wide with walls 30 cm high; this testing area was divided into a grid of 66 equally sized squares. Ink foot printing and careful observation allowed the number of crossed squares to be recorded for each mouse over a 1 min period.

Acknowledgments

We are grateful to Arthur Beaudet (Baylor College of Medicine, Houston) for making his transgenic facility available for these studies. We thank Shayam Sharan, Glenn I. Fishman, and Ting-Fang Tsai for their suggestions; Jason Chiu, Teresa A. Milner, and Jody Culkin for technical assistance; Craig Gerard for sharing unpublished data; and Peter Brophy, David Colman, John Hemperly, and Jim Trimmer for kindly providing antibodies. This work was supported by the Howard Temin Career Development Award from the National Cancer Institute (KO1-CA 78437) and Mount Sinai School of Medicine start up funds (M.A.B.), NIH grants NS38208 (J.L.S.), NS37475 (J.R.), and NMSS grant RG2539 (J.R.). J.C.R and W.C. are Medical Scientist Trainees supported by NIH grant 5T32 GM07308 from NIGMS. H.J.B. is an investigator of the Howard Hughes Medical Institute.

Received April 6, 2001; revised April 10, 2001.

References

Andres, K.H. (1965). Über die Feinstruktur besonderer Einrichtungen in markhaltigen Nervenfasern des Kleinhirns der Ratte. Z. Zellforsch. Mikrosk. Anat. *65*, 701–712.

Bargmann, W., and Lindner, E. (1964). Über den Feinbau des Nebennierenmarkes des Igels (*Erinaceus europaeus L*). Z. Zellforsch. Mikrosk. Anat. *64*, 868–912.

Baumgartner, S., Littleton, J.T., Broadie, K., Bhat, M.A., Harbecke, R., Lengyel, J.A., Chiquet-Ehrismann, R., Prokop, A., and Bellen, H.J. (1996). A Drosophila neurexin is required for septate junction and blood-nerve barrier formation and function. Cell *87*, 1059–1068.

Bellen, H.J., Lu, Y., Beckstead, R., and Bhat, M.A. (1998). Neurexin IV, caspr and paranodin—novel members of the neurexin family: encounters of axons and glia. Trends Neurosci. *21*, 444–449.

Bennett, V., and Lambert, S. (1999). Physiological roles of axonal ankyrins in survival of premyelinated axons and localization of voltage-gated sodium channels. J. Neurocytol. *28*, 303–318.

Berglund, E.O., Murai, K.K., Fredette, B., Sekerkova, G., Marturano, B., Weber, L., Mugnaini, E., and Ranscht, B. (1999). Ataxia and abnormal cerebellar microorganization in mice with ablated contactin gene expression. Neuron *24*, 739–750.

Bhat, M.A., Philp, A.V., Glover, D.M., and Bellen, H.J. (1996). Chromatid segregation at anaphase requires the *barren* product, a novel chromosome-associated protein that interacts with topoisomerase II. Cell *87*, 1103–1114.

Bhat, M.A., Izaddoost, S., Lu, Y., Cho, K.O., Choi, K.W., and Bellen, H.J. (1999). Discs Lost, a novel multi-PDZ domain protein, establishes and maintains epithelial polarity. Cell *96*, 833–845.

Bonini, J.A., and Steiner, D.F. (1997). Molecular cloning and expression of a novel rat CC-chemokine receptor (rCCR10rR) that binds MCP-1 and MIP-1beta with high affinity. DNA Cell Biol. *16*, 1023–1030.

Bosio, A., Bussow, H., Adam, J., and Stoffel, W. (1998). Galactosphingolipids and axon-glial interaction in myelin of the central nervous system. Cell Tissue Res. *292*, 199–210.

Bunge, R.P., Bunge, M.B., and Bates, M. (1989). Movements of the Schwann cell nucleus implicate progression of the inner (axon-related) Schwann cell process during myelination. J. Cell Biol. *109*, 273–284.

Coetzee, T., Fujita, N., Dupree, J., Shi, R., Blight, A., Suzuki, K., and Popko, B. (1996). Myelination in the absence of galactocerebroside and sulfatide: normal structure with abnormal function and regional instability. Cell *86*, 209–219.

Collinson, J.M., Marshall, D., Gillespie, C.S., and Brophy, P.J. (1998). Transient expression of neurofascin by oligodendrocytes at the onset of myelinogenesis: implications for mechanisms of axon-glial interaction. Glia *23*, 11–23.

Davis, J.Q., Lambert, S., and Bennett, V. (1996). Molecular composition of the node of Ranvier: identification of ankyrin-binding cell adhesion molecules neurofascin (mucin+/third FNIII domain-) and NrCAM at nodal axon segments. J. Cell Biol. *135*, 1355–1367.

Dupree, J.L., and Popko, B. (1999). Genetic dissection of myelin galactolipid function. J. Neurocytol. *28*, 271–279.

Dupree, J.L., Coetzee, T., Blight, A., Suzuki, K., and Popko, B. (1998). Myelin galactolipids are essential for proper node of Ranvier formation in the CNS. J. Neurosci. *18*, 1642–1649.

Dupree, J.L., Girault, J.A., and Popko, B. (1999). Axo-glial interactions regulate the localization of axonal paranodal proteins. J. Cell Biol. *147*, 1145–1152.

Einheber, S., Zanazzi, G., Ching, W., Scherer, S., Milner, T.A., Peles, E., and Salzer, J.L. (1997). The axonal membrane protein Caspr, a homologue of neurexin IV, is a component of the septate-like paranodal junctions that assemble during myelination. J. Cell Biol. *139*, 1495–1506.

Faivre-Sarrailh, C., and Rougon, G. (1997). Axonal molecules of the immunoglobulin superfamily bearing a GPI anchor: their role in controlling neurite outgrowth. Mol. Cell. Neurosci. *9*, 109–115.

Faivre-Sarrailh, C., Gauthier, F., Denisenko-Nehrbass, N., Le Bivic, A., Rougon, G., and Girault, J.A. (2000). The glycosylphosphatidyl inositol-anchored adhesion molecule F3/Contactin is required for surface transport of Paranodin/Contactin-associated protein (caspr). J. Cell Biol. *149*, 491–502.

Homey, B., Wang, W., Soto, H., Buchanan, M.E., Wiesenborn, A.,

Catron, D., Muller, A., McClanahan, T.K., Dieu-Nosjean, M.C., Orozco, R., et al. (2000). Cutting edge: the orphan chemokine receptor G protein-coupled receptor-2 (GPR-2, CCR10) binds the skin-associated chemokine CCL27 (CTACK/ALP/ILC). J. Immunol. *164*, 3465–3470.

Jarmin, D.I., Rits, M., Bota, D., Gerard, N.P., Graham, G.J., Clark-Lewis, I., and Gerard, C. (2000). Cutting edge: identification of the orphan receptor G-protein-coupled receptor 2 as CCR10, a specific receptor for the chemokine ESkine. J. Immunol. *164*, 3460–3464.

Koch, T., Brugger, T., Bach, A., Gennarini, G., and Trotter, J. (1997). Expression of the immunoglobulin superfamily cell adhesion molecule F3 by oligodendrocyte-lineage cells. Glia *19*, 199–212.

Melendez-Vasquez, C.V., Rios, J.C., Zanazzi, G., Lambert, S., Bretscher, A., and Salzer, J.L. (2001). Nodes of Ranvier form in association with ERM-positive Schwann cell processes. Proc. Natl. Acad. Sci. USA *98*, 1235–1240.

Menegoz, M., Gaspar, P., Bert, M.L., Galvez, T., Burgaya, F., Palfrey, C., Ezan, P., Arnos, F., and Girault, J.-A. (1997). Paranodin, a glycoprotein of neuronal paranodal membranes. Neuron *19*, 319–331.

Missler, M., and Südhof, T.C. (1998). Neurexins: three genes and 1001 products. Trends Genet. *14*, 20–26.

Peles, E., Nativ, M., Lustig, M., Grumet, M., Schilling, J., Martinez, R., Plowman, G.D., and Schlessinger, J. (1997). Identification of a novel contactin-associated transmembrane receptor with multiple domains implicated in protein-protein interactions. EMBO J. *16*, 978–988.

Peles, E., and Salzer, J.L. (2000). Molecular domains of myelinated axons. Curr. Opin. Neurobiol. *10*, 558–565.

Poliak, S., Gollan, L., Martinez, R., Custer, A., Einheber, S., Salzer, J.L., Trimmer, J.S., Shrager, P., and Peles, E. (1999). Caspr2, a new member of the neurexin superfamily, is localized at the juxtaparanodes of myelinated axons and associates with potassium channels. Neuron *24*, 1037–1047.

Raine, C.S. (1982). Differences between the nodes of Ranvier of large and small diameter fibres in the P.N.S. J. Neurocytol. *11*, 935–947.

Rios, J.C., Melendez-Vasquez, C.V., Einheber, S., Lustig, M., Grumet, M., Hemperly, J., Peles, E., and Salzer, J.L. (2000). Contactin-associated protein (Caspr) and contactin form a complex that is targeted to the paranodal junctions during myelination. J. Neurosci. *20*, 8354–8364.

Robertson, J.D. (1957). The ultrastructure of nodes of Ranvier in frog nerve fibers. J. Physiol. *137*, 8–9.

Rosenbluth, J. (1995). Glial membranes and axoglial junctions. In Neuroglia, H. Kettenmann and B.R. Ransom, eds. (New York: Oxford University Press), pp. 613–633.

Rudenko, G., Nguyen, T., Chelliah, Y., Sudhof, T.C., and Deisenhofer, J. (1999). The structure of the ligand-binding domain of neurexin Ibeta: regulation of LNS domain function by alternative splicing. Cell *99*, 93–101.

Sharan, S.K., Morimatsu, M., Albrecht, U., Lim, D.S., Regel, E., Dinh, C., Sands, A., Eichele, G., Hasty, P., and Bradley, A. (1997). Embryonic lethality and radiation hypersensitivity mediated by Rad51 in mice lacking Brca2. Nature *386*, 804–810.

Tait, S., Gunn-Moore, F., Collinson, J.M., Huang, J., Lubetzki, C., Pedraza, L., Sherman, D.L., Colman, D.R., and Brophy, P.J. (2000). An oligodendrocyte cell adhesion molecule at the site of assembly of the paranodal axo-glial junction. J. Cell Biol. *150*, 657–666.

Talts, J.F., Andac, Z., Gohring, W., Brancaccio, A., and Timpl, R. (1999). Binding of the G domains of laminin alpha1 and alpha2 chains and perlecan to heparin, sulfatides, alpha-dystroglycan and several extracellular matrix proteins. EMBO J. *18*, 863–870.

Thullier, F., Lalonde, R., and Lestienne, F. (1999). Effects of dopaminergic agents and of an NMDA receptor antagonist on motor coordination in Lurcher mutant mice. Pharm. Biochem. Behav. *63*, 213–219.

Ward, R.E., Lamb, R.S., and Fehon, R.G. (1998). A conserved functional domain of Drosophila coracle is required for localization at the septate junction and has membrane-organizing activity. J. Cell Biol. *140*, 1463–1473.

Wang, W., Soto, H., Oldham, E.R., Buchanan, M.E., Homey, B., Catron, D., Jenkins, N., Copeland, N.G., Gilbert, D.J., Nguyen, N., et al. (2000). Identification of a novel chemokine (CCL28), which binds CCR10 (GPR2). J. Biol. Chem. *275*, 22313–22323.